Eco-Engineered Ag-Fe_2O_3 Hybrid nanoparticles: biofabrication and solar photocatalytic performance in environmental water purification

Buthainah Saeeb Saleh[1] Hind Khader Abbas[2] Suha mohammed abbas[3] Mohammed F. Abood[4]

[1,2,3]Anbar Education Directorate, Iraq
[4]University of Anbar, College of Education for Pure Sciences

Email: buthena145@gmail.com

Abstract

Sustainable treatment of wastewater is a big environmental problem. It needs better. Eco-friendly nanomaterials. This study wanted to make a silver-iron oxide (Ag-Fe2O3) bimetallic nanocomposite. The method used a way. For the time it used an aqueous extract from the leaves of the Black nightshade plant (Solanum nigrum L.) as a reducing agent and biostabilizer. The study also checked how good the nanocomposite was at breaking down crystal violet dye. The method involved making the nanomaterial with a process. It then used techniques to study the nanocomposite. These techniques included UV-Vis spectroscopy, FTIR, XRD, FESEM and TEM. The method also looked into the photodegradation speed. It also studied how the amount of pollutant and the type of source like UVA or sunlight affected the process. The results showed that the nanoparticles were almost spherical. Their average size was 26.49 nm. This proved that the silver and magnetic iron oxide (γ-Fe□O□) had crystal phases. The composite worked well. It removed 96.5% of the crystal violet dye under UVA light. It removed 94.5% under sunlight. This was at 10 mg L□¹ over 60 minutes. The study, on how the reaction happened showed it followed a quasi-first-order model. The better performance came from the combination of silver and iron oxide. This combination helped reduce the recombination of charges. It also helped absorb visible light. So the method based on plants offers a cheap way. It creates efficient nanocatalysts. These can be used for cleaning water with the help of the sun.

Keywords: Green Synthesis , Solanum nigrum L., Nano Oxide, Ag-Fe2O3 , photocatalytic Degradation , Crystal Violet

Introduction

Wolfberry (*Solanum nigrum* L.), a perennial herbaceous shrub belonging to the nightshade family (Solanaceae), represents a vital and sustainable resource due to its wide geographical distribution and rich content of phytochemicals. Extracts from this plant, particularly those from the leaves, possess high efficiency in reducing and fixing metals thanks to their high content of polyphenols, flavonoids, alkaloids, and tannins [1,2]. In recent years, these bio-extracts have garnered significant attention in green nanotechnology for the synthesis of metal nanoparticles as an environmentally friendly, low-cost, and non-toxic alternative to traditional physical and chemical methods. These latter methods consume high energy and require the use of hazardous chemical primers and reducers, negatively impacting the environment and limiting

ISSN 2072-3857

the bioapplications of the resulting particles.[3] . Bio-components extracted from the leaves of Solanum nigrum L. play a dual role in the green manufacturing process; These biomolecules act as natural reducing agents, capable of converting metal ions from their soluble oxidized states into zero-valence nanoparticles via redox reactions catalyzed by hydroxyl bonds.[4] Furthermore, these biomolecules act as capping agents, surrounding the formed nanoparticle surfaces. This biocapacitance prevents particle aggregation due to van der Waals forces, ensuring long-term colloidal stability and controlling particle size and morphology—factors that directly govern surface activity and catalytic efficiency[5].

Silver-iron oxide (Ag-Fe) bimetallic nanoparticles (Ag-FeO) are of exceptional importance in environmental applications due to the synergistic effects arising from the integration of these two components into a single hybrid nanostructure. [6,7] Iron oxide phases (such as hematite α-Fe□O_3 or magnetite γ-Fe_2 O_3) provide an abundant, chemically stable, and low-toxicity carrier platform with optimal band gap energy properties ranging from 2.0 to 2.3 eV. This narrow band gap makes them highly efficient at absorbing light within the visible spectrum, which is essential for solar photocatalytic applications and the generation of active free radicals responsible for breaking down pollutants . [8,9]

By introducing a small fraction of silver (“Ag”) and grafting it onto the iron oxide (Fe□O□) matrix, a so-called “catalytic serum” is formed. Silver atoms act as electron sinks for photoexcited electrons due to their surface plasmon resonance (SPR) properties [10]. This structure effectively prevents the rapid recombination of free electrons and positive holes generated when iron oxide is exposed to light, thus prolonging the lifetime of active charges and increasing the production of hydroxyl radicals (·"OH") and superoxide radicals (·"O"-2^-). The synergistic mechanism enhances the catalytic capacity of the nanosystem and reduces the high economic cost by decreasing the amount of pure silver used and replacing it with cheaper and more readily available iron oxides[11], the increasing pollution of water sources by industrial waste of chemically stable organic dyes, such as crystal violet, poses a significant environmental and health risk due to these aromatic compounds' resistance to natural biodegradation and their high spectral stability [12,13]. Crystal violet dye is a rigorous model for evaluating the efficiency of novel photocatalysts, as breaking its complex bonds requires a catalytic system capable of generating a high oxidation potential to rupture the aromatic rings and convert them into harmless compounds, water, and carbon dioxide [14] The importance of green manufacturing of silver-iron (Ag-Fe) hybrid nanocomposites and their environmental applications is highlighted [15], reported the preparation of Ag-Fe□O□ nanoparticles with a unique spider-thorn-like shape and an average size of approximately 1 nanometer, using an extract from the leaves of the plant *Sosauria obvalata.* These results support the conclusions of current research regarding the pivotal role of green manufacturing methods and the type of plant extract in determining the morphological and structural properties of hybrid compounds, which directly affect their catalytic efficiency. Regarding the application efficiency under natural solar irradiance, [16]. developed a bimetallic system of Ag-Fe

ISSN 2072-3857

particles using palm bud extract, where the system achieved a green malachite removal rate of 11.23% at a concentration of 10 mg/L within 180 minutes. Regarding the stability of colloids and their electrokinetic properties, investigated the properties of Ag/Fe□O□ nanoparticles synthesized using beetroot extract, where the surface charge measured by zeta potential recorded a relatively low value (-0.2 mV>.[18]

The study also aims to characterize the structural, optical, and morphological properties of the resulting particles, evaluate their catalytic efficiency, and investigate the reaction kinetics of the photo-induced removal of the crystal violet dye under visible light irradiation conditions, to offer a promising and sustainable environmental solution for wastewater treatment.

Materials and methods

Materials

The chemical precursors utilized for the nanoparticle synthesis included analytical-grade iron (III) nitrate nonahydrate [$Fe(NO_3)_3 \cdot 9H_2O$, 98%] and silver nitrate ($AgNO_3$, 99%), both procured from Sigma-Aldrich (ACS reagent grade). Sodium hydroxide (NaOH, 98%) and ethanol (96%), purchased from Prochima Sigma, were employed without further purification. Hydrochloric acid (HCl, reagent grade, 36.5–38%) was obtained from Honeywell. The model dye, Crystal Violet (AR grade), was supplied by TMMEDIA. Throughout all experimental stages, including solution preparation and washing, distilled water (DW) was strictly used as the primary solvent. To prepare the bio-extract, fresh leaves of the black eggplant (*Solanum nigrum* L) were collected from its natural habitat in Diyala Governorate, located in eastern Iraq.

Plant Preparation and Extraction

Fresh leaves of *S. nigrum* L. were harvested during the pre-flowering stage, thoroughly washed with distilled water (DW) to remove debris, and dried shade. The dried leaves were ground into a fine powder, and 30 g of the powder was suspended in 500 mL of DW. The mixture was heated at 80–90 °C for 30 min to extract the bioactive metabolites. After cooling, the solution was filtered through Whatman No. 4 filter paper. The resulting aqueous extract (pH 5.1) was stored in the dark at 4 °C for subsequent synthesis[18].

Synthesis of Iron-Silver Oxide (Ag-Fe□O□) Nanoparticles:

Iron-silver oxide (Ag-Fe_2O_3) nanoparticles were synthesized using a modified biosynthetic protocol. Briefly, 100 mL of aqueous extract of black nightshade (Solanum nigrum L.) leaves was added dropwise via burette to an Erlenmeyer flask containing 1.0 g of hydrated ferric nitrate ($Fe(NO□)□ \cdot 9H□O$) and 0.1 g of silver nitrate ($AgNO□$) dissolved in 100 mL of distilled water. The reaction mixture was maintained at 70–80 °C with continuous stirring at 1000 rpm for 2 hours. During the process, the pH of the solution was maintained at 7.0 by the strategic, then add hydrochloric acid (less than 1 M) and sodium hydroxide in a gradual and controlled manner. solution. The resulting precipitate of nanoparticles was collected, thoroughly washed, and stored in a controlled environment before undergoing analysis and photocatalytic applications[19,20].

ISSN 2072-3857

Characterization of Ag-Fe_2O_3 NPs

The physicochemical attributes of the biogenic Ag-Fe_2O_3 nanoparticles were comprehensively analyzed using various analytical techniques. Optical properties of colloidal suspensions were evaluated via UV-Vis spectroscopy (Shimadzu UV-1900-i) between 200 and 800 nm, while solid bandgap estimations were determined using Diffuse Reflectance Spectroscopy (UV-DRS, Thermo Scientific Evolution 201). The structural integrity and crystallinity were assessed by Powder X-ray Diffraction (PXRD, Malvern Panalytical Empyrean) using Cu Kα radiation ($\lambda = 0.15406$ nm) across 2θ angles ranging from 20° to 80°. Furthermore, ATR-FTIR spectroscopy (Shimadzu IRSpirit-X) was utilized within the 400--4000 cm^{-1} range to identify the plant-derived functional groups responsible for reduction and stabilization. Morphological features and elemental compositions were investigated through FE-SEM (JEOL JSM-7200F) coupled with EDX, alongside TEM (JEOL JEM-F200) to determine particle size distribution from sonicated ethanolic suspensions. Finally, the surface charge and colloidal stability were measured via zeta potential analysis using a NICOMP 380 ZLS analyzer in ultra-pure water[22].

Photocatalytic Degradation and Kinetics

The photocatalytic efficiency of the synthesized Ag-Fe_2O_3 nanoparticles were evaluated through the degradation of Crystal Violet dye under visible light irradiation, carefully accounting for photolysis and dark adsorption controls. The degradation efficiency ($R\%$) was calculated using the following equation:

$$R\% = \frac{C_0 - C_f}{C_0} \times 100$$

Where C_0 and C_f represent the initial and final dye concentrations (mg L^{-1}) at $t = 0$ and $t = 60$ min, respectively. To understand the reaction dynamics, the degradation kinetics were modeled utilizing the non-linear pseudo-first-order (PFO) kinetic equation:

$$\frac{C_t}{C_0} = e^{-k_{app} t}$$

Where C_t is the dye concentration at any given irradiation time t, and k_{app} (min^{-1}) denotes the apparent rate constant[23,24]

Photocatalytic Degradation Study

The photocatalytic performance of the biogenic Ag-Fe_2O_3 nanoparticles were evaluated under solar irradiation. Solar degradation experiments were systematically conducted around solar noon (approximately 12:00 local time) to ensure maximum and consistent solar irradiance. The initial concentration of the target pollutant (Crystal Violet, mg L^{-1}) was monitored over time, and the resulting data were fitted to the non-linear pseudo-first-order (PFO) kinetic model to determine the apparent rate constant (k_{app}), allowing a precise quantification of the nanoparticle-mediated light-induced degradation efficiency[25].

Results and discussion

UV-Vis Spectroscopy Analysis

The biogenic synthesis of Ag-Fe_2O_3 NPs were initially evidenced adding the

ISSN 2072-3857

aqueous ***S. nigrum*** extract, indicating metal ion reduction. UV-Vis spectrophotometric profiles (Fig. 1) confirmed nanoparticle formation. The crude exhibited a prominent absorption peak at 267 nm due to $\pi \rightarrow \pi^*$ electronic transitions within aromatic phenolic and flavonoid rings. The hybrid Ag-Fe_2O_3 NPs displayed enhanced UV-region absorption compared to individual iron oxide nanoparticles (IONPs) and a distinct peak at 274 nm, typical for iron oxide nanostructures (Fe_xO_y literature peaks at 270, 277, and 294 nm). Interestingly, the characteristic metallic silver surface plasmon resonance (SPR) band around 420 nm was suppressed. This masking effect is attributed to the high iron-to-silver precursor mass ratio (10: 1), promoting iron-dominant surface coverage, plasmon damping, or a core–shell architecture where the silver core is encapsulated by the Fe_2O_3 matrix.

Despite the obscured absorption SPR band, the photoluminescence (PL) emission spectrum of the hybrid Ag-Fe_2O_3 NPs (Fig. 2ii) revealed strong optical activity. The profile displays a sharp, well-defined blue emission peak centered at 408 nm, reaching a maximum intensity of approximately 970 nm, which highlights the efficient radiative recombination of photo-generated charge carriers crucial for photocatalyst.

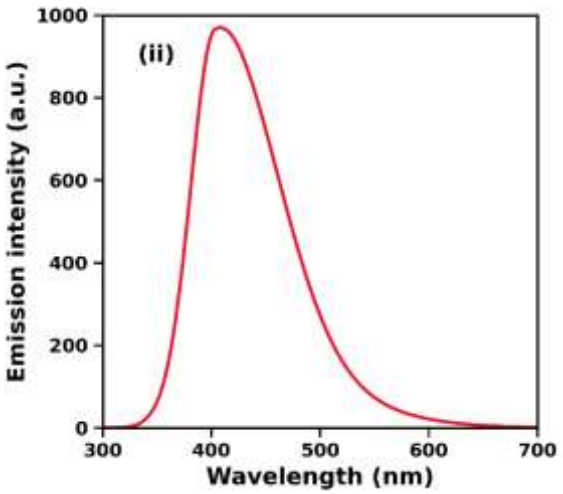


Fig. 1: UV-Vis absorption spectra of the biogenic *S. nigrum* extract extract, the as-synthesized hybrid Ag-Fe_2O_3 NPs, and their monometallic counterparts (IONPs and AgNPs.

Fourier-transform infrared spectroscopy (FT-IR)

The FT-IR spectrum was recorded to identify the functional groups in the *Solanum nigrum* L. leaf extract responsible for the bioreduction and stabilization of the Ag-Fe_2O_3 nanocomposite (Fig. 2). A broad absorption band centered around 3415 cm^{-1} is assigned to the stretching vibrations of hydroxyl (O-H) groups present in polyphenols and flavonoids, as well as adsorbed water molecules. The weak absorption peaks observed at approximately 2920 cm^{-1} and 2850 cm^{-1} correspond to asymmetric and symmetric C-H stretching vibrations of aliphatic hydrocarbons.

The prominent peak at 1635 cm^{-1} is attributed to the stretching vibration of carbonyl (C=O) or aromatic C=C bonds, confirming the participation of

ISSN 2072-3857

phytoconstituents in stabilizing the metal surface. Bands in the region of 1380--1050 cm^{-1} represent C-O and C-N stretching vibrations of biomolecules. Significantly, new absorption bands appearing in the fingerprint region between 530 cm^{-1} and 630 cm^{-1} correspond to the characteristic lattice vibration modes of Fe-O bonds in maghemite (γ-Fe_2O_3) and metal–ligand interactions with silver. These spectral features collectively confirm that the bioactive compounds of *Solanum nigrum* L. effectively acted as dual reducing and capping agents in the formation of stable Ag-Fe_2O_3 nanoparticles

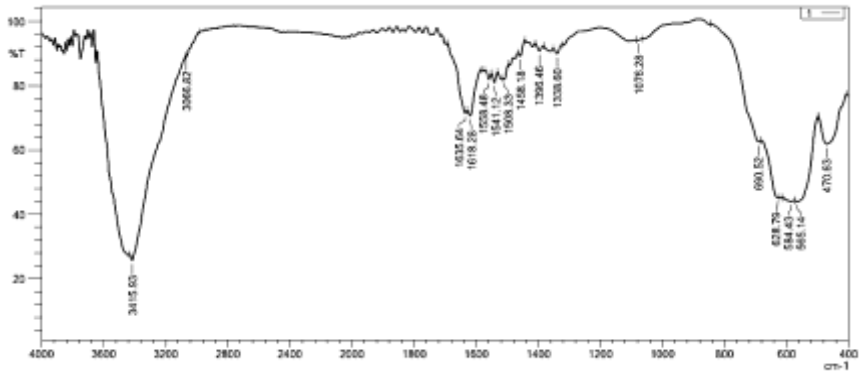


Fig. 2: FTIR Spectra of the aqueous extract of *S. nigrum and* Ag-Fe_2O_3 NPs.

X-ray di□raction (XRD)

The crystal structure and phase purity of the biosynthesized Ag-Fe□O□ nanocomposite were investigated using X-ray diffraction (Figure 3). The diffraction pattern shows distinct peaks indicative of both metallic silver (Ag) and hematite (α-Fe□O□) phases. The diffraction peaks observed at 2θ values of 38.1°, 44.3°, 64.4°, and 77.4° correspond to the (111), (200), (220), and (311) crystal planes of face-centered cubic silver (FCC) (JCPDS No. 04-0783). In addition, the peaks at 24.1°, 33.1°, 35.6°, 40.8°, and 54.0° are attributed to levels (012), (104), (110), (113), and (116) of α-Fe□O□ orthorhombic hematite (JCPDS No. 33-0664). The average crystal size calculated using the Scherrer equation is approximately 26.5 nm, which agrees well with the crystal size distribution analysis using transmission electron microscopy (TEM).

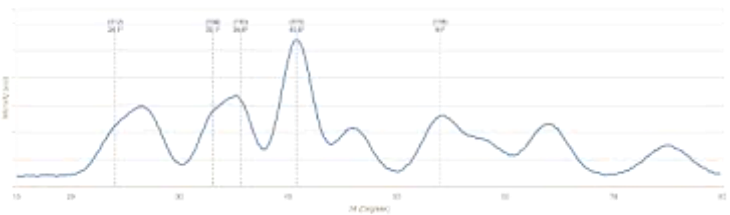


Fig. 3: XRD Pattern of the green synthesized Ag-Fe_2O_3 NPs before and after photocatalysis.

Emission scanning electron microscopy (FESEM) analysis

The surface morphology and microstructure of the biosynthesized Ag-Fe□O□ nanocomposite were characterized using field-emission scanning electron microscopy (FE-SEM) and (Figure 4). FE-SEM images show quasi-spherical nanoparticles with a relatively homogeneous distribution, along with slight agglomeration attributed to the high surface energy and magnetic dipole interactions inherent in hematite (α-Fe□O□) nanostructures. The relatively small average size suggests that the environmentally friendly synthesis method promoted efficient nucleation and controlled growth; however, the observed dispersal indicates the inherent variability of the reduction process mediated by phytochemicals.

Bioactive compounds, including phenols, flavonoids, and proteins found in plant extracts such as *S. nigrum*, may act as reducing and stabilizing agents, but with weaker stabilizing properties than synthetic surfactants; thus, some partial aggregation and average dispersal variability are expected [26].

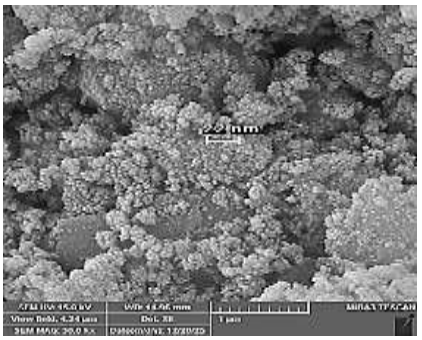


Fig. 4 SEM images at different magnifications of Ag-Fe_2O_3

.

Transmission electron microscopy (TEM)

TEM technology reveals silver and iron nanoparticles in order to obtain essential information such as shape imaging, crystallinity, dispersion, and accurate estimation of nanoparticle size[22].

TEM analysis confirms the quasi-spherical shape and nanoscale dimensions of the hybrid composite. The particle size distribution plot extracted from the TEM images indicates an average particle diameter of 26.49 nm, which shows excellent agreement with the crystalline domain size (26.5 nm) calculated from X-ray diffraction using the Scherrer equation. The close agreement between the particle size measured by TEM and the crystalline domain size measured by X-ray diffraction confirms the homogeneity of the dispersion of the synthetic nanoparticles. The stability of the synthesized Ag-Fe□O□ nanoparticles was evaluated by measuring their zeta potential (Figure 5). The nanocomposite exhibited a negative surface charge, primarily attributed to the adsorption of anionic bioactive groups (such as hydroxyl and carboxyl groups from the black nightshade leaf extract) onto the nanoparticle surface. This negative surface charge provides strong electrostatic repulsion between adjacent particles, effectively preventing agglomeration and ensuring high colloidal stability in aqueous media[27], each particle

ISSN 2072-3857

of NPs was measured three times, the size distribution analysis in Figure 5 shows that the prepared green nanoparticles had a predominant average diameter of 26.49 nanometers.

using *Salvia o□cinalis* leaf extract; they reported polydisperse near-spherical NPs that have an average diameter of 27.48 ± 6.88 nm [24]. Fig. 7b represents one single isolated nanoparticle of 27.284 ± 1.66 nm, showing a dark core and a thin lighter shell.

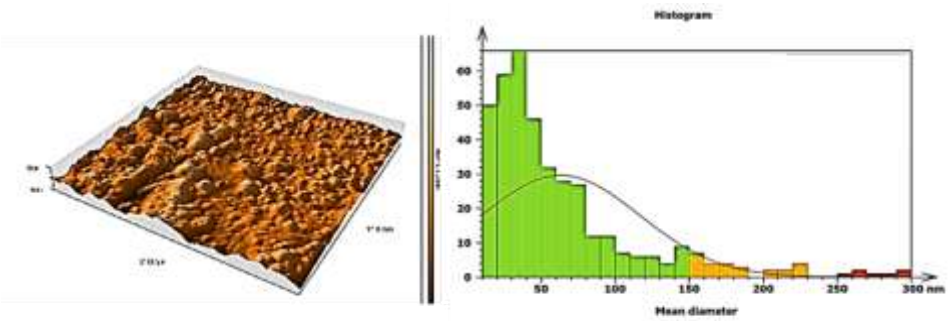


Fig. 5: TEM images of Ag-Fe_2O_3 NPs at different magnifications and their size distribution.

Most systems in Ag/Ag2O/g-Fe_2O_3 assays are heterogeneous, potentially consisting of core-shell structures,silver-iron anocomposites, or discrete silver-iron nanoparticles, depending on the accuracy and methods of plant synthesis [28]. For example, core-shell structures have been used with S. persica and Gardenia jasminoides. Iron-iron-silver nanoparticles in the form of dumbbells have also been obtained [29].from The composite nanostructures were reported in the two references that synthesized Fe2O3/Ag nanocomposites using *Aloe vera* and Buddleja *lindleyana*[30], each the crystallite size calculated from XRD was smaller than the TEM estimated average; This difference may be due to the detection of small crystals by X-ray diffraction, and the rest of the spectroscopic tests only, with the omission of larger aggregates, and the possibility that the nanoparticles are polycrystalline or form aggregates of polycrystalline nanoparticles [31,32].

Effect of initial dye concentration on photosynthetic performance

Catalytic photolysis was studied as a function of the initial dye concentration (10–50 mg/L) under both UVA and natural solar irradiance, as summarized in Fig. 7. A clear and consistent decline in removal efficiency was observed with increasing pollutant load for both light sources: under UVA irradiation, the removal percentage decreased from 96.5% at 10 mg L□¹ to 79.2% at 50 mg L□¹, while under solar irradiation it dropped from 94.5% to 77.8% over the same concentration range. This inverse relationship between initial concentration and degradation efficiency is a well-documented feature of heterogeneous photocatalysis and can be rationalized on two complementary grounds. First, the number of catalytically active sites on the Ag–Fe□O□ surface remains

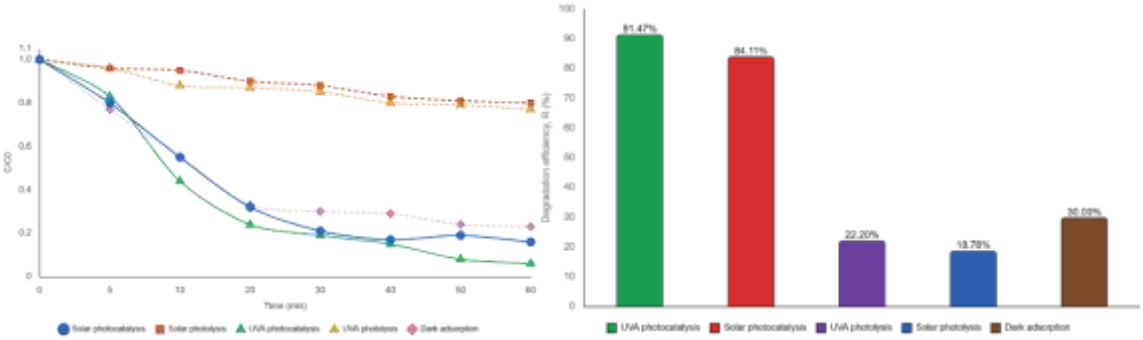
fixed throughout the reaction, whereas the number of dye molecules requiring degradation scales with concentration; Consequently, the active sites become progressively saturated, lowering the fractional (though not necessarily the absolute) rate of removal. Second, at higher dye loadings a greater fraction of incident photons is absorbed directly by the dye molecules in solution rather than by the catalyst surface—an inner-filter effect—which curtails the generation of electron–hole (e^-/h^+) pairs and, in turn, the population of reactive oxidizing species. The concentration dependence observed here is consistent with pseudo-first-order Langmuir–Hinshelwood kinetics, commonly used to describe such heterogeneous photocatalytic systems.

A comparison of the two irradiation sources reveals that UVA light consistently afforded slightly higher removal efficiencies than solar irradiation, a gap that widened noticeably at 30 mg L^{-1} (91.4% versus 82.1%). This discrepancy reflects the differing spectral characteristics of the two sources the UVA lamp delivers a stable, narrow-band emission that closely matches the band-gap energy of α-Fe_2O_3, whereas solar radiation is distributed across a much broader spectrum dominated by visible and infrared wavelengths, with only a minor UV component whose intensity further fluctuates with atmospheric conditions, solar angle, and time of exposure. Despite this spectral mismatch, the relatively small performance gap between the two sources is noteworthy, as it indicates that the catalyst retains substantial activity under visible-dominated solar light. This behavior is attributed to the incorporation of silver nanoparticles onto the Fe_2O_3 surface, which extends light harvesting into the visible region through localized surface plasmon resonance (LSPR) and simultaneously acts as an electron sink that suppresses charge-carrier recombination—both effects enhancing photocatalytic efficiency under the UV-poor conditions typical of natural sunlight.

To confirm that the decolorization resulted from true heterogeneous photocatalytic in Fig 6 and tab. 1 reaction rather than physical adsorption or direct photolysis, control experiments were performed at 30 mg/L under four distinct conditions: dark/no catalyst, dark/catalyst, light/no catalyst, and light/catalyst (Figure 6). In the dark with the catalyst present, a slight decrease in concentration (15.1%) was observed over 30 minutes, consistent with the equilibrium of physical adsorption and decomposition of crystalline violet at the active sites of silver oxide and ferric trioxide. Similarly, irradiation in the absence of the catalyst (photolysis) resulted in very little decomposition (<5%), confirming the stability of the photochemically photostatically. In stark contrast, the simultaneous presence of light and the catalyst resulted in the highest decomposition efficiency (91.4% under UVA irradiation and 82.1% under sunlight at a concentration of 30 mg/L). These basic controls definitively confirm that catalytic photolysis—driven by photogenerated free radical species (•OH and $•O_2^-$)—is the dominant removal mechanism. Under these conditions, photon absorption by Ag–Fe_2O_3 generates electron–hole pairs that react with adsorbed water and dissolved oxygen to yield reactive oxygen species (notably hydroxyl radicals, •OH, and superoxide anions,

ISSN 2072-3857

O□•□), which attack the chromophoric groups of the CV molecule and drive its progressive mineralization into simpler intermediates and ultimately CO□ and H□O.



a b

Fig. 6: (a) Photocatalytic degradation of crystal violet (CV) using Ag-Fe_2O_3 NPs under UVA and Solar irradiation: (b) removal efficiency of CV at varying concentrations and light sources.

Taken together, these results support the conclusion that the biosynthesized Ag–Fe□O□ nanoparticles combine high photocatalytic activity with an extended visible-light response, positioning them as promising, low-cost candidates for the solar-driven remediation of dye-contaminated wastewater—offering a sustainable alternative to energy-intensive UV-based treatment systems.

Table 1: effect of irradiation (dark *vs.* light) and catalyst presence (photocatalysis *vs.* photolysis) .

Initial Concentration, C (mg/L)	Solar Irradiation (R%)	UVA Irradiation (R%)
10	94.502	96.513
20	94.454	94.073
30	82.138	91.445
50	77.753	79.246

c

Metallic nanoparticles are among the most effective tools for removing organic dyes from contaminated water thanks to their unique physicochemical properties that distinguish them from conventional bulk materials [33]. These properties include a relatively large surface area relative to their size, high catalytic activity, and the ease with which their surface properties and structure can be modified [34]. Research has shown that these particles are widely used in water treatment, medicine, energy generation, and bioremediation, and that

they act as effective catalysts in reduction reactions Among metallic nanoparticles, silver nanoparticles (AgNPs) stand out due to their excellent antimicrobial and catalytic properties. Silver nanoparticles synthesized using kiwi fruit extract (*Actinidia deliciosa*) demonstrated the ability to completely decompose methylene blue within 33 minutes in the presence of a catalyst[35], while nanoparticles synthesized from Barkia roxburghi leaf extract achieved complete decomposition of both methylene blue and rhodamine B in just 12 minutes[36]. These results strongly support the trend toward green manufacturing of metallic nanoparticles using plant extracts, as this approach combines high catalytic efficiency with environmental sustainability and avoids the use of toxic chemical reagents employed in conventional manufacturing methods.

Similarly, transition metal oxides such as zinc oxide (ZnO) are attracting considerable attention due to their large surface area, non-toxicity, structural stability, high photosensitivity, high reactivity, and low cost; they are considered effective photocatalysts for dye removal [37]. For example, ZnO nanoparticles prepared from an extract of Artocarpus heterophyllus leaves achieved complete degradation of rose bengal dye within one hour, while biosynthesized nanoparticles from Aspergillus sp. showed good efficiency in degrading methylene blue dye [38]. Results for zirconium oxide nanoparticles prepared from Lagerstroemia speciosa leaves indicate their ability to degrade methyl orange dye by up to 94.5%, a percentage very close to that observed in the current study for the Ag-Fe2O3 catalyst at low concentrations. This reinforces the confidence that transition metal oxide-based nanocatalysts, whether single- or bi-component, offer a promising platform for treating industrial wastewater contaminated with dyes [39]. The catalytic performance of these materials is further enhanced by the combination of two different nanometals in a single structure. Studies have shown that bimetallic nanoparticles such as Fe–Ni are capable of decomposing the Orange G dye into intermediate products such as naphtholamine and aniline derivatives [40], while composite nanoparticles such as CuO–ZnO have demonstrated superior catalytic performance in the decomposition of the Rhodamine B dye compared to each component alone [41]. This synergy between two different metallic components is explained by the improved separation of electrical charges and the reduced likelihood of electron-hole pair recombination. This same principle explains the remarkable improvement in the catalytic performance of the Ag–Fe□O□ nanoparticles studied in this research, where silver acts as the site for collecting excited electrons, while ferric oxide provides the basic spectral response[42,43].

The role of noble metals in general, such as silver, gold, and platinum, in enhancing the photocatalytic properties of semiconductors when deposited on their surface cannot be overlooked. They act as electron traps, preventing the rapid recombination of electron-hole pairs, thus extending the lifetime of charge carriers and increasing the efficiency of redox reactions [44]. These noble metals also exhibit localized surface plasmon resonance (LSPR), which significantly enhances light absorption in the visible range [45]. This same mechanism explains the relative improvement in the performance of the Ag-Fe_2O_3 catalyst under solar irradiation in the current study.

It is also worth noting that incorporating metallic nanoparticles with basic semiconductor oxides such as titanium dioxide is a common strategy for extending the spectral response towards visible light. Silver-doped compounds on the surface of TiO2 have shown a marked improvement in the decomposition of synthetic dyes under visible light [46], and a green-processed ZnO/TiO2 nanocomposite has achieved efficient removal of cationic and anionic dyes under solar irradiation[47]. Taken together, these results support the hypothesis that doping transition metal oxides with noble metal nanoparticles, as in the Ag-Fe_2O_3 catalyst used in this study, represents an effective and viable approach to overcoming the spectral

ISSN 2072-3857

limitations of conventional semiconductors with their wide energy gaps.

Finally, the use of magnetic nanoparticles, such as those prepared from Moringa oleifera extract, opens up further possibilities for improving the recoverability and reuse of the catalyst from an aqueous medium using an external magnetic field [48]. This is an important practical advantage to consider in future applications of iron oxide-based catalysts like Ag-Fe_2O_3, as it combines high catalytic efficiency with easy separation and the sustainability of repeated use without significant loss of efficiency.

Conclusion

This study demonstrates the efficiency of a green and sustainable manufacturing approach in developing a silver-iron oxide (Ag-Fe_2O_3) bimetallic nanocomposite using an aqueous extract of leaves (Solanum nigrum L.) as a reducing agent and biostabilizer for the first time. Structural and morphological characterization assays (such as XRD and TEM) showed the formation of quasi-spherical nanoparticles with an average crystalline size of 26.49 nm, with confirmed fusion of silver-iron oxide (Fe_2O_3) phases and the presence of phenolic and plant compounds that coated the surface and protected the particles from agglomeration. Environmentally, the hybrid material exhibited superior photodegradation efficiency of the water-polluting crystal violet (CV) dye within 60 minutes. The removal rate reached 96.5% under UVA irradiation and 94.5% under natural sunlight at a concentration of 10 mg L□¹. The kinetic study confirmed that the reaction followed a quasi-first-order model. This outstanding performance is attributed to the synergistic effect between silver and iron oxide; silver acts as an electron trap, limiting the recombination of photocharges, while simultaneously enhancing visible light absorption via surface plasmon resonance. These results present a promising and sustainable platform offering a low-cost, environmentally friendly solution for industrial wastewater treatment using solar energy.

Conflicts of interest:

There are no conflicts to declare.

Data availability

References

[1] Mohyuddin, A., Kurniawan, T. A., Khan, Z. U. D., Nadeem, S., Javed, M., Dera, A. A., ... & Saeed, S. (2022). Comparative insights into the antimicrobial, antioxidant, and nutritional potential of the Solanum Nigrum complex. *Processes*, *10*(8), 1455.

[2] Dai, H., Wei, S., Twardowska, I., Hou, N., & Zhang, Q. (2022). Cosmopolitan cadmium hyperaccumulator Solanum nigrum: Exploring cadm Souza, L. D. S. D., Andrade, B. O., & Stehmann, J. R. (2023). An overview on studies of species complexes in Solanaceae. *Acta Botanica Brasilica*, *37*, e20230032. ium uptake, transport and physiological mechanisms of accumulation in different ecotypes as a way of enhancing its hyperaccumulative capacity. *Journal of Environmental Management*, *320*, 115878.

[3] Abd-Elhamed, W., Mohamed, A. A., Saad, Z. H., Hassanien, S. E. S. I., Salem, M. Z., & El-Hefny, M. (2025). Green synthesis of silver nanoparticles mediated by Solanum nigrum leaf extract and their antifungal activity against pine pathogens. *Scientific Reports*, *15*(1), 35025.

[4] Gharari, Z., Sadeghinia, H., & Hanachi, P. (2026). In vitro Evaluation of the Antioxidant and Anti-cancer Potential of Gold Nanoparticles Fabricated from Extracts of Regenerated Solanum nigrum. *Nanochemistry Research*, *11*(2), 234-244.

[5] Saranya, T., Ramya, S., Kavithaa, K., Paulpandi, M., Cheon, Y. P., Harysh Winster, S., ... & Narayanasamy, A. (2023). Green synthesis of selenium nanoparticles using solanum nigrum fruit extract and its anti-cancer efficacy against

triple negative breast cancer. *Journal of Cluster Science*, *34*(4), 1709-1719.

[6] Al-Ghamdi, M. M. A., Alsheheri, S. Z., Alezi, D., & Zaheer, Z. (2026). Synthesis, characterization, and visible light induced photocatalytic activity of iron doped silver (Ag@ Fe) nano-photocatalyst for the degradation of rhodamine B. *Journal of Molecular Structure*, 145629.

[7] Lekoui, F., Hassani, S., Garoudja, E., Amrani, R., Filali, W., Sifi, O., & Oussalah, S. (2023). Elaboration and characterization of pure ZnO, Ag: ZnO and Ag-Fe: ZnO thin films: Effect of Ag and Ag-Fe doping on ZnO physical properties. *Revista mexicana de física*, *69*(5), 0-0.

[8] Kotolevich, Y., Khramov, E., Sánchez-López, P., Pestryakov, A., Zubavichus, Y., Antúnez-Garcia, J., & Petranovskii, V. (2023). Formation of Ag-Fe bimetallic nano-species on mordenite depending on the initial ratio of components. *Materials*, *16*(8), 3026.

[9] Patel, B., Choudhary, N., Dudhagara, D., Shahid, M., Syed, R., Yadav, V. K., ... & Patel, A. (2025). Green synthesis of Ag–Fe bimetallic nanoparticles using fungal filtrates: unlocking multifunctional medical and environmental applications. *RSC advances*, *15*(3), 1565-1575.

[10] DVORETSKAYA, A., ANIKANOVA, L., SUDZILOVSKAYA, T., & DVORETSKII, N. (2025). FROM CHEMISTRY TOWARDS TECHNOLOGY STEP-BY-STEP. *FROM CHEMISTRY TOWARDS TECHNOLOGY STEP-BY-STEP Учредители: Ярославский государственный технический университет*, *6*(2), 112-119.

[11] He, T., Zhao, Y., Benetti, D., Moss, B., Tian, L., Selim, S., ... & Durrant, J. R. (2024). Facet-engineered BiVO4 photocatalysts for water oxidation: lifetime gain versus energetic loss. *Journal of the American Chemical Society*, *146*(39), 27080-27089.

[12] Kamal, A. B., Hassane, A. M., An, C., Deng, Q., Hu, N., Abolibda, T. Z., ... & Gomaa, H. (2025). Developing a cost-effective and eco-friendly adsorbent/photocatalyst using biomass and urban waste for crystal violet removal and antimicrobial applications. *Biomass Conversion and Biorefinery*, *15*(7), 10089-10107.

[13] Sharma, P., Kar, S., Sahu, M., & Ganguly, M. (2025). Copper-based nanoparticles for the removal of the crystal violet dye via degradation and adsorption: a comparative account. *RSC advances*, *15*(34), 27995-28020.

[14] Shabna, S., Singh, C. J. C., Dhas, S. D. S. J., Jeyakumar, S. C., & Biju, C. S. (2024). An overview of prominent factors influencing the photocatalytic degradation of cationic crystal violet dye employing diverse nanostructured materials. *Journal of Chemical Technology & Biotechnology*, *99*(5), 1027-1055.

[15] Kadkhodayan, H., & Alizadeh, T. (2025). Construction of novel Fe6W18O70/In2WO6/Ag-doped g-C3N4 ternary heterojunction photocatalyst for photodegradation of various environmental contaminants. *International Journal of Environmental Science and Technology*, *22*(1), 133-152.

[16] Langa, C., Mabuba, N., Mahlaule-Glory, L. M., Motaung, D. E., Tetana, Z., & Hintsho-Mbita, N. C. (2025). XRD intensity variations in recovered nanomaterials. *International Journal of Environmental Analytical Chemistry*, 1–31.

[17] Habeeba, U., & Raghavendra, N. (2024). Green synthesis of metal-based nanoparticles using plant extracts. *Discover Chemistry*, *1*, Article 45.

[18] Melese Birru, E., Adela Alemu, M., Tsegaw Weredekal, A., Belay Asrie, A., & Geta Mengistie, M. (2022). Antimalarial activity of crude extract and solvent

ISSN 2072-3857

fractions of leaves of Solanum nigrum L.(Solanaceae) against plasmodium berghei in mice. *Evidence‐Based Complementary and Alternative Medicine*, *2022*(1), 3426175.

[19] El-Khateeb, A. Y. (2025). Biosynthesis of Ag, Fe_2O_3, and hybrid Ag/Fe_2O_3 nanoparticles using clove (Syzygium aromaticum): A study on phytochemicals, antioxidant capacity, and antibacterial properties. *Journal of Agriculture, Food and Environment| ISSN (Online Version): 2708-5694*, *6*(2), 30-43.

[20] Saleem, H., Ozdemir, F. A., Qunlu, L., Hassan, S. W., Nawab, R., Haroon, U., ... & Munis, M. F. H. (2026). Biogenic Fe_2O_3 nanoparticles enhance carotenoid pathway gene expression and suppress verticillium root rot in marigold (Tagetes erecta). *BMC Plant Biology*, *26*(1), 1091.

[21] Fatima, S., & Arshad, N. (2024). Ocimum Tenuiflorum-mediated Biosynthesis of Silver Iron (Ag/Fe) Bimetallic Nanoparticles and Evaluation of their Antiglycation and Biocompatibility Activities. *PAKISTAN JOURNAL OF BIOCHEMISTRY AND MOLECULAR BIOLOGY*, *57*(2), 6-19.

[22] Al-Ghamdi, M. M. A., Alsheheri, S. Z., Alezi, D., & Zaheer, Z. (2026). Synthesis, characterization, and visible light induced photocatalytic activity of iron doped silver (Ag@ Fe) nano-photocatalyst for the degradation of rhodamine B. *Journal of Molecular Structure*, 145629.

[23] Sudhakar, C., Selvam, K., Poonkothai, M., & Ranjitha, S. (2024). Biomimetic synthesis of Ag@ Fe bimetallic nanoparticles from Palmyra sprouts extract and their antibacterial, photocatalytic degradation of malachite green. *Inorganic Chemistry Communications*, *161*, 112132.

[24] Idris, D. S., & Roy, A. (2024). Antioxidant and dye degradation activity of green synthesized silver-iron oxide (Ag-Fe2O3) bimetallic nanoparticles. *Nano-Structures & Nano-Objects*, *38*, 101142.

[25] Roy, A., Kunwar, S., Bhusal, U., Idris, D. S., Alghamdi, S., Chidambaram, K., ... & Roy, A. (2024). Dye degradation activity of biogenically synthesized Cu/Fe/Ag trimetallic nanoparticles. *Green Processing and Synthesis*, *13*(1), 20230267.

[26] Asad, S., Murad, W., Anwar, N., Asad, K., Khan, M. S., Azizi, S., & Maaza, M. (2026). Synthesis and Characterization of Ag–Fe Bimetallic Nanoparticles and Nanocomposites (Alloys and Core–Shells) for Photocatalytic Degradation of Bromophenol Blue Dye Using Grewia optiva Leaf Extract. *Asia‐Pacific Journal of Chemical Engineering*, e70222.

[27] Sarani, M., Hamidian, K., Barani, M., Adeli‐Sardou, M., & Khonakdar, H. A. (2023). α‐Fe2O3@ Ag and Fe3O4@ Ag core‐shell nanoparticles: green synthesis, magnetic properties and cytotoxic performance. *ChemistryOpen*, *12*(6), e202200250.

[28] Gharad, R., & Maity, C. (2026). Supramolecular Vesicles as Nanoreactors Enable Green Synthesis of Ultrasmall Silver Oxide Nanoparticles for Visible-Light Photocatalysis. *Nanoscale Advances*.

[29] Sun, M., Cai, J., Yang, K., Zhang, W., Sun, M., Meng, H., ... & Rao, B. (2025). Green Synthesis of Carbon Quantum Dots from Gardenia Jasminoides for the Selective Detection of Fe3+ Ions and Cell Imaging. *ACS Applied Bio Materials*, *8*(10), 9245-9253.

[30] Aswathy, V. P., Bains, A., Sridhar, K., Chawla, P., Sharma, M., Ali, N., ... & Goksen, G. (2024). Nano polysaccharides derived from aloe vera and guar gum as a potential fat replacer for a promising approach to healthier cake production. *International Journal of Biological Macromolecules*, *267*, 131431.

[31] Bassani, C. L., Van Anders, G., Banin, U., Baranov, D., Chen, Q., Dijkstra, M., ... & Travesset, A. (2024). Nanocrystal assemblies: Current advances and open

problems. *ACS nano*, *18*(23), 14791-14840.

[32] Hurley, M. J., Tanner, C. P., Portner, J., Utterback, J. K., Coropceanu, I., Das, A., ... & Teitelbaum, S. W. (2024). In situ coherent x-ray scattering reveals polycrystalline structure and discrete annealing events in strongly coupled nanocrystal superlattices. *Physical Review Research*, *6*(2), 023119.

[33] Choi, W. S., & Lee, H. J. (2022). Nanostructured materials for water purification: adsorption of heavy metal ions and organic dyes. *Polymers*, *14*(11), 2183.

[34] Boucetta, R. N., Khelfaoui, M., Ammouchi, N., Boucetta, S., Khelifi, M. N., Can, E., ... & Djazi, F. (2026). Highly efficient photocatalytic degradation of dyes and anticancer activity of eco-friendly synthesized Ag/Ag2O/γ-Fe2O3 nanoparticles using Cistus monspeliensis leaf extract. *RSC advances*, *16*(7), 5915-5931.

[35] Kassem Agha, M., Maatouk, B., Mhanna, R., & El-Dakdouki, M. H. (2024). Catalytic degradation efficacy of silver nanoparticles fabricated using Actinidia deliciosa peel extract. *Journal of Nanomaterials*, *2024*(1), 8813109.

[36] Pérez-Flores, J. G., García-Curiel, L., Pérez-Escalante, E., Contreras-López, E., Rodríguez-Serrano, G. M., Rivera-Arredondo, M., ... & Guerrero-Solano, J. A. (2026). Alcalase for Food-Protein-Derived Bioactive Peptides: Trends, Gaps, and Translational Opportunities. *Macromol*, *6*(1), 16.

[37] Li, H., Naeem, U., Li, P. J., Wu, L. J., Yue, H. W., Alshoaibi, A., ... & Mohamad, A. A. (2025). Structural Analysis by X- Ray Diffraction Technique of Transition Metal Doped Zinc Oxide and Its Applications in Energy Storage Systems: A Critical Review. *International Journal of Energy Research*, *2025*(1), 2587682.

[38] Ugendar, C. M., Pani, A. S., Rambabu, K., Naina, Singh, P., Sivakumar, K., ... & Prasad, C. (2026). A TD-DFT Exploration and Artocarpus heterophyllus Plant Leaf Extract-Based Decolorization of Methylene Blue. *Water, Air, & Soil Pollution*, *237*(3), 147.

[39] Alsultan, H. K. A. A. K., & Guda, M. A. (2024). Green Synthesis of Zirconium Oxide Nanoparticles and their Effect on Inhibition Growth of Bacteria. *Journal of Physico-Chemical Material (JPCM)*, *1*(1).

[40] Xu, D., Cao, X., Zhou, J., Lin, Z., Wang, J., Han, J., ... & Xu, D. (2025). Analysis of microstructure properties of Ni-Fe MOFs and their influence on selective recognition of single and binary dye systems. *npj Clean Water*, *8*(1), 35.

[41] Xiao, L., Ma, W., Li, H., Yu, Y., Liu, S., Zeng, X., ... & Yang, C. Y. (2025). Synthesis and Efficacy of ZnO-CuO Piezoelectric Catalysts: A Cost-Effective Catalysts for Efficient Degradation of Organic Pollutants and Antibacterial in Water. *Catalysis Letters*, *155*(8), 264.

[42] Mishra, R., Meher, A., Sahu, S. K., Panda, N. R., & Sahu, D. (2026). Ag- Doped α-Fe2O3 Nanoparticles: Synthesis, Characterization, and Photocatalytic Degradation of Rhodamine B. *ChemistrySelect*, *11*(17), e07557.

[43] Zouari Ahmed, R., Laouini, S. E., Salmi, C., Bouafia, A., Meneceur, S., Mohammed, H. A., ... & Abdullah, J. A. A. (2025). Green synthesis of α-Fe2O3 and α-Fe2O3@ Ag NC for degradation of rose Bengal and antimicrobial activity. *Biomass Conversion and Biorefinery*, *15*(1), 255-269.

[44] Goncearenco, E., Morjan, I. P., Dutu, E., Scarisoreanu, M., Fleaca, C., Gavrila-Florescu, L., ... & Balint, I. (2022). The effect of noble metal addition on the properties of oxide semiconductors nanoparticles. *Journal of Solid State Chemistry*, *307*, 122817.

[45] Habibi Masheli, M., Eyvazi, S., Aghdaee, M., & Amjad, J. M. (2023). LSPR of nanoparticles inside strong absorbent

medium. *The Journal of Physical Chemistry C*, *127*(49), 23696-23705.

[46] Bibi, S., Shah, S. S., Muhammad, F., Siddiq, M., Kiran, L., Aldossari, S. A., ... & Sarwar, S. (2023). Cu-doped mesoporous TiO2 photocatalyst for efficient degradation of organic dye via visible light photocatalysis. *Chemosphere*, *339*, 139583.

[47] Anil, K., & Surenjan, A. (2024). Green synthesis, characterisation, and performance evaluation of ZnO/TiO2 nanocomposite for cationic and anionic dye removal from aqueous solutions under solar irradiation. *Water Practice & Technology*, *19*(3), 824-838.

[48] Pattnaik, A., Poonia, A. K., & Ghosh, P. (2025). Ultrasonication-assisted green synthesis of Moringa oleifera-mediated defect-rich BFO photocatalyst: Kinetic insights and economic feasibility. *Journal of Environmental Chemical Engineering*, 120444.

ISSN 2072-3857